

INTERNAL INTERFACES IN TURBULENT BOUNDARY LAYERS OVER SURFACES WITH SMOOTH-TO-ROUGH TRANSITION OF WALL ROUGHNESS

R. Jason Hearst

Department of Energy & Process Engineering
Norwegian University of Science & Technology
Trondheim, NO-7491, Norway
jason.hearst@ntnu.no

Bharathram Ganapathisubramani

University of Southampton
Southampton, SO17 1BJ, United Kingdom
g.bharath@southampton.ac.uk

ABSTRACT

The development of internal layers after a smooth-to-rough step change in wall topology is investigated over a $\sim 11\delta_0$ field-of-view. Independent realisations of the flow field are captured with particle image velocimetry at $Re_\tau \approx 1100$ for two downstream roughness topologies. A criterion to instantaneously identify the position of the inner layer is developed based on tracking how uniform momentum zone modal velocities change across the step change in roughness. The mean location of this instantaneous internal layer is shown to agree with prior estimations of the development of an equilibrium layer immediately adjacent to the wall, which has historically been identified via inflections in the mean velocity profile. It is demonstrated that the height of the downstream roughness impacts the mean growth of the internal layer as well as the fluctuations in its position and the conditional velocity jump across it. The latter two statistics are not directly measurable without the technique introduced herein.

INTRODUCTION

When flow encounters a step change in wall roughness, an internal boundary layer is formed near the wall. This internal layer grows with streamwise position and eventually dominates the entire boundary layer, returning it to equilibrium with the new boundary conditions (Antonia & Luxton, 1971a, 1972). This idea is illustrated for a smooth-to-rough (S \rightarrow R) transition in Fig. 1, where δ_0 is the thickness of the incoming boundary layer and y_i is the height of the internal layer, which is a function of the streamwise position, x . Over the years, several different approaches have been used to identify the internal layer. For instance, Antonia & Luxton (1971a, 1972) and Hanson & Ganapathisubramani (2016) tracked the internal layer by identifying where the slope in U/U_∞ versus $y^{1/2}$ changed (where the y -direction is wall-normal). In contrast, Bou-Zeid *et al.* (2004) and Dupont & Brunet (2009) tracked the internal layer by identifying the height where the local gradient $\partial U/\partial y$ was equal to

the streamwise averaged value of the same gradient. Even more simply, Pendergrass & Arya (1984), Cheng & Castro (2002) and Lee (2015) tracked the inner layer by linking its position with the height where U/U_∞ becomes 99% of its value upstream of the change in surface roughness. These various techniques have reported a range of growth rates of the inner layer after a smooth-to-rough transition, typically of the form $y_i \propto x^\alpha$, with α ranging from 0.2 (Lee, 2015) to 0.9 (Dupont & Brunet, 2009). Rouhi *et al.* (2019) recently performed direct numerical simulations (DNS) over both a smooth-to-rough and a rough-to-smooth step change in wall topology, and reviewed the internal layer tracking techniques available in the literature. They found that the significant scatter in inner layer growth reported by previous studies was at least in part due to the different methods used to track the inner layer evolution. Rouhi *et al.* (2019) commented that the idea that is most in keeping with the concept of an internal layer is that proposed by Elliott (1958) who associated the inner layer with changes in the slope of U^+ versus $\ln y^+$, where y^+ is used to identify normalisation by inner (or wall) units, i.e., $y^+ = yU_\tau/\nu$, $U^+ = U/U_\tau$ where U_τ is the friction velocity.

Despite the wide array of criteria used to track the inner layer, they share a commonality: they are all based on the mean flow profile. Historically, this was one of the only sets of information available to researchers as wind tunnel tests would have been performed with hot-wire anemometry and field tests with cup anemometers. However, with the advent of techniques that allow us to interrogate an instantaneous velocity field, e.g., particle image velocimetry (PIV)

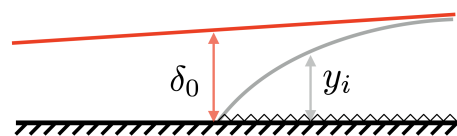


Figure 1. Schematic of the growth of the inner boundary layer after a smooth-to-rough transition in surface topology.

or DNS, we can be more critical of how the inner layer re-surfing from a change in surface topology is both tracked and generally understood.

If we take a step back and consider what is happening in the flow as it transitions from a smooth to a rough surface, we take note that the flow perceives a change in friction over the transition resulting in a new, larger velocity deficit region next to the wall. An example of this is provided in Fig. 2. The mean location of the upper edge of the deficit layer is what the mean profile techniques are meant to track, as this initially manifests as an inflection in the mean velocity profile. However, the ideas diverge here. In the mean profile, the inflection point will increase in wall-normal position until it dominates the boundary layer and establishes a new equilibrium with the rough wall. Meanwhile, the deficit region will never grow to occupy the entire boundary layer, but rather will initially grow into existence, and then match the growth of δ once the flow has reached an equilibrium state with the new wall condition.

At present there is no methodology for identifying the inner layer instantaneously, and thus one must be developed. It is well established that a canonical turbulent boundary layer is instantaneously populated by a layered structure of velocity regions with approximately uniform momentum, referred to as uniform momentum zones (UMZs). The UMZs are separated by shear events that are responsible for a significant amount of the production in the boundary layer (Meinhart & Adrian, 1995; de Silva *et al.*, 2016). Given that the internal boundary layer is traditionally associated with an inflection in the mean velocity profile, which identifies an area of high mean shear, it suggests that the UMZ structure could potentially facilitate instantaneous tracking of the growth of the internal layer. We thus apply a UMZ-based methodology for identifying the velocity region associated with the step change in roughness, and track the evolution of this interface. The new methodology is applied to two downstream surface roughnesses and is compared with the traditional mean velocity-based approaches. To track the evolution over a significant region, independent PIV snapshots are acquired over a $\sim 11\delta_0$ field-of-view (FOV).

EXPERIMENTAL DETAILS

PIV measurements were performed over a S→R step change in wall roughness in the $0.6\text{ m} \times 0.9\text{ m} \times 4.5\text{ m}$ suction wind tunnel at the University of Southampton. A turbulent boundary layer was formed over an artificial floor placed inside the wind tunnel (Fig. 3(a)). The flow was initially tripped with a zig-zag roughness element and then allowed to evolve over a smooth wall for 2.45 m before the abrupt transition to roughness. Two types of roughness were investigated: (i) an isotropic, non-Gaussian, abrasive ‘grit’ pattern with a maximum height of 2 mm, and (ii) an aluminum diamond-shaped ‘mesh’ mounted to the wall with a maximum height of 4 mm (Fig. 3(b)). The grit roughness is sheets of 16-gauge industrial open-type silicon carbide abrasive, similar to that used by Birch & Morrison (2011). The elements of the mesh roughness have a cross-section of $2.35\text{ mm} \times 1.5\text{ mm}$, and the diamonds are 30.5 mm wide and 11.7 mm long. The diamonds are oriented such that their longest dimension is across the wind tunnel span. Both roughness geometries are ‘upstanding’ using the terminology of Antonia & Luxton (1971b), which means they are placed above the surface of the smooth wall. The roughness patterns themselves are described in

greater detail by Hanson & Ganapathisubramani (2016). Both roughness patterns extend 0.90 m downstream of the transition.

PIV images were acquired simultaneously with four LaVision ImagerProLX 16 mega-pixel cameras oriented to capture an extended planar streamwise FOV. The cameras were equipped with Nikon Nikkor 200 mm lenses. Particles with a diameter of approximately $1\text{ }\mu\text{m}$ were produced by an industrial smoke machine, and were illuminated by two synchronised Litron Nano PIV lasers (Nd-YAG, 532 nm, 200 mJ per pulse). The final FOV was $520\text{ mm} \times 90\text{ mm}$ (length \times height). The images were stitched together by using the calibration geometry and making manual adjustments (on the scale of $\sim 1\text{ mm}$) to ensure that the instantaneous structures and floor were properly aligned after processing. A linear weighting was used to blend the overlapped region between images. Images were processed using LaVision DaVis version 8.2 using square windows of decreasing size and an overlap of 50%. A minimum of 3000 image pairs were acquired for both test cases. All fields were corrected for pixel-locking on a vector-by-vector basis (Hearst & Ganapathisubramani, 2015).

Incoming flow conditions for both cases are provided in Table 1. In general, the experiment was designed to keep the development Reynolds number constant at $Re_x = U_\infty x/\nu \approx 1.6 \times 10^6$. The Reynolds number based on the friction velocity ($Re_\tau = U_\tau \delta/\nu$) and the momentum thickness ($Re_\theta = U_\infty \theta/\nu$ where θ is the momentum thickness) are provided in Table 1. Here, the subscript \cdot_0 is used to denote an incoming quantity, calculated for the acquired field that is $x/\delta_0 < -1.5$. The incoming boundary layer thickness (δ_0) is estimated using the composite multi-variable fit of Rodríguez-López *et al.* (2015), and is approximately 13% higher than δ_{99} in the present study. The same fitting technique also provides an estimate of U_τ , which was within 5% of U_τ estimated from the velocity gradient and the Reynolds shear stress $\langle uv \rangle$ at the wall; thus, an average of the estimates was used for U_τ . In effect, the incoming flow from both cases is the same within the uncertainty of the experiment and thus any downstream change after the S→R transition is a result of the change in surface roughness.

Table 1. Incoming flow parameters for both test cases.

Case	U_∞ [m/s]	$Re_{\tau,0}$	$Re_{\theta,0}$	θ_0 [mm]	δ_0 [mm]
Mesh	10.0	1140	3300	5.0	46
Grit	9.9	1130	3130	4.8	45

MEAN PROFILE ANALYSIS

As a benchmark, it is important to understanding the evolution of the mean velocity fields for the two cases and identify if they differ. In their study, Rouhi *et al.* (2019) tracked the inner layer using a variety of mean profile analyses to comment on their similarities and differences. For brevity, we focus on the mean profile analysis of Elliott (1958) as this was the one found to be “more consistent”

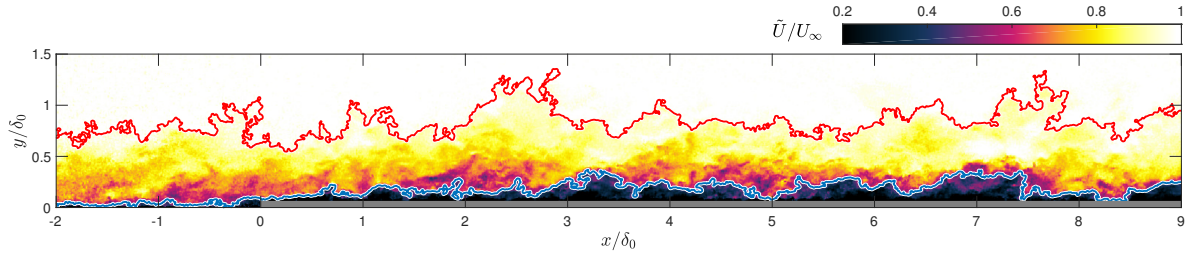


Figure 2. Instantaneous streamwise velocity field above a smooth-to-rough transition in wall surface. The red line represents the instantaneous position of the turbulent/non-turbulent interface identified by thresholding equation 1, and the blue line represents the internal layer identified using the instantaneous approach described herein. The portrayed field uses the ‘mesh’ roughness.

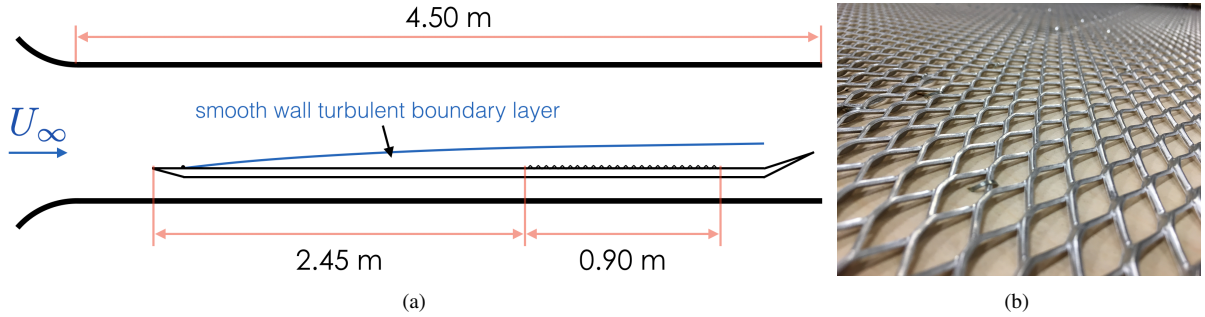


Figure 3. Experimental configuration. (a) Schematic of the wind tunnel and artificial floor configuration (not to scale). (b) Photograph of mesh roughness. The maximum height of the roughness was $4 \text{ mm} = 0.09\delta_0$.

with the ideas of an inner boundary layer (Rouhi *et al.*, 2019). In this approach, inflection points in the $U^+ - \ln y^+$ curve are sought. In practice this is done by identifying local maxima and minima in $\partial U^+ / \partial \ln y^+$ and finding the intersection point between different linear sections of the semilog curve. The process is illustrated in Fig. 4, where three local maxima/minima are identified in the gradient, and these are then plotted on the U^+ -curve along with the slope at each point. This identifies three approximately linear regions, and their intersections are the inflection points.

To produce the curves from which the inflection points are found, the velocity and wall-normal position are normalised by the incoming friction velocity ($U_{\tau,0}$) upstream of the transition. This is done because it is difficult to estimate U_{τ} locally over the roughness. Nonetheless, as observed by Rouhi *et al.* (2019), the normalisation of the curve in Fig. 4 does not impact the identification of inflection points. In order to produce profiles that are smoother, and thus have less noise in the gradient estimation, we produce a profile by averaging over a $0.3\delta_0$ window in the streamwise direction. The gradient is then estimated from a basic forward difference because the spacing between points is not even when transformed to $\ln y^+$ -space. The calculated gradient is then smoothed over seven points using a Hanning window.

A few observations can be made from Fig. 4. The first is that there appears to be three approximately linear regions in the velocity profile, with two inflection points in the range typically occupied by the log region for a smooth wall. The upper of these two inflection points is the one most commonly associated with the inner boundary layer, c.f., Elliott (1958); Rouhi *et al.* (2019). This approach has not been previously used to identify the ‘equilibrium layer’ whereby the flow closest to the wall has reached its new equilibrium state with the changed boundary condition (Cheng & Castro, 2002; Lee, 2015), but given the resolution and size of

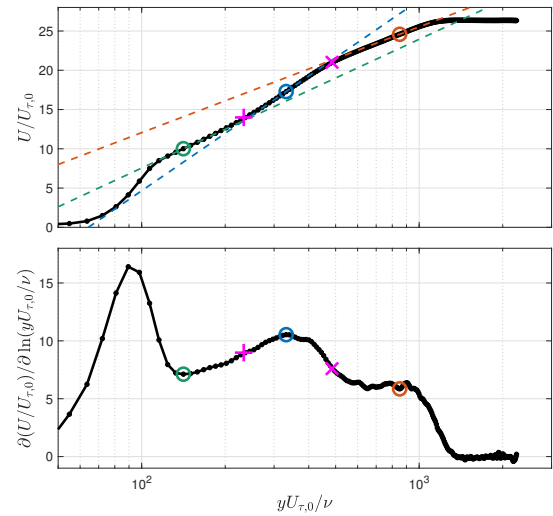


Figure 4. Mean-profile-based inner boundary layer detection method based on the approach of Elliott (1958) and performed in the manner of Rouhi *et al.* (2019). The particular profile shown here is for the mesh roughness at $x/\delta_0 = 3$ downstream of the S→R transition. The circles represent the positions of local maxima and minima, and the dashed lines shown the slope at these positions. The + and × identify the inflection points in the mean velocity profile based on the intersection points of the regions of constant slope.

the layer in the present study for the mesh roughness, it appears that we are able to track this lower inflection point as well.

The evolution of the two inflection points for both

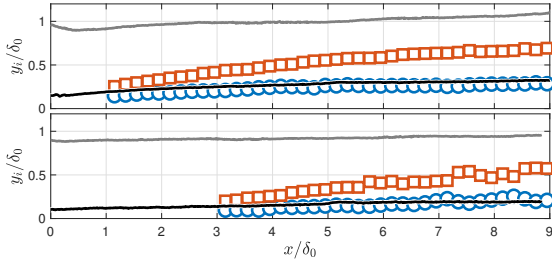


Figure 5. Streamwise evolution of inner layers over a S→R transition in wall condition for the (top) mesh and (bottom) grit roughness. The grey line represents δ_{99} ; the black line represents the mean location of the instantaneous inner layer; (\square) is the upper inflection point in the mean profile; (\circ) is the lower inflection point in the mean profile. The aspect-ratio of the figure is meant to roughly show the wall-normal and streamwise evolution in relative terms; the wall-normal direction is amplified by a factor of 2.

roughness geometries is provided in Fig. 5 along with the mean position of the instantaneous inner layer (to be discussed in subsequent sections) and the position of δ_{99} (given for reference). Note that for the mesh case, $\delta_{99} < \delta_0$ initially, as expected upstream of the step change in roughness, but by $x/\delta_0 = 9$, δ_{99} has grown such that it is larger than the initial boundary layer thickness. We track the evolution of δ_{99} rather than δ because the composite approach to estimate δ is not well-established over roughness. Notice that for the grit roughness, which is less rough, $\delta_{99} < \delta_0$ for the entire FOV, suggesting that the growth rate of δ is larger for the rougher (mesh) surface.

Focussing on the inflection points for the mesh case, fitting a power-law of the form $y_i \propto x^\alpha$ to $x/\delta_0 > 1$ yields $\alpha = 0.48$ for the upper inflection points and $\alpha = 0.30$ for the lower inflection point. If the upper inflection point is the boundary of the inner boundary layer, then this estimate is near $\alpha = 0.58$ estimated by Rouhi *et al.* (2019) in a channel flow with a lower Re_{τ_0} and a different roughness. The estimate here is also in about the centre of the scatter presented in the literature from the various methods.

At this stage, we do not have a strong estimate of the growth rate of the inflection points for the grit roughness. There is visibly more scatter in Fig. 5 for the grit case, which results from the changes in the velocity profile being more subtle for the grit geometry which has a lower roughness height. This is also why estimates of the layers are only made for $x/\delta_0 > 3$, because the inflection points cannot be accurately located for $x/\delta_0 < 3$ as the boundary layer has not yet visibly responded to the change in roughness. This in itself is telling as it suggests that the grit has less of an impact on the flow.

DETECTING INTERNAL LAYERS

Our primary interest is in determining if the instantaneous structure of the wall-bounded flow is somehow related to the mean profile analyses of the previous section. To do this, we use a UMZ-based approach whereby the UMZs that exist downstream of the S→R transition are compared to those that exist upstream.

The first step in accurately identifying UMZs in the boundary layer is detecting and excluding velocity vectors associated with the free-stream flow (de Silva *et al.*, 2016,

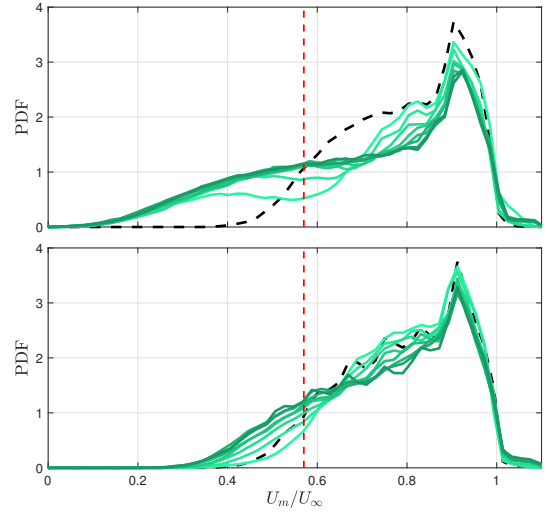


Figure 6. Probability density functions of the modal velocities for the (top) mesh and (bottom) grit cases. The black dashed line is for the upstream window $-2.00 \leq x/\delta_0 \leq -1.75$, and the green solid lines represent $0.25\delta_0$ windows at $x/\delta_0 = 1$ through 8 from lightest to darkest. The vertical red dashed line represents the inner layer threshold velocity set to $U/U_\infty = 0.57$.

2017). We do this here by isolating a band upstream of the S→R transition, $-2.00 \leq x/\delta_0 \leq -1.75$, and using it to determine a suitable threshold based on the kinetic energy deficit,

$$\tilde{k} = 100 \times \frac{1}{9U_\infty} \sum_{m,n=-1}^1 [(\tilde{U}_{m,n} - U_\infty)^2 + (\tilde{V}_{m,n})^2], \quad (1)$$

that separates the instantaneous vortical flow in the boundary layer from the irrotational free-stream flow, i.e., the turbulent/non-turbulent interface (TNTI) (Chauhan *et al.*, 2014). In equation 1, a tilde, $\tilde{\cdot}$, is used to denote an instantaneous quantity. In this case, the threshold is found to be $k_{th} = 0.20$ and is applied to the entire flow field. This threshold produces an approximately Gaussian distribution of the TNTI location and an error function in the intermittency profile, as expected (Chauhan *et al.*, 2014). The most likely position of the TNTI is $\sim 0.72\delta_0$ and this is also where the intermittency crosses 50% for both cases.

UMZs upstream and downstream of the step change in roughness were identified with the histogram approach established by Meinhart & Adrian (1995) and developed further by de Silva *et al.* (2016). In short, an instantaneous probability density function (PDF) of the velocities beneath the TNTI was computed for a region that was $0.25\delta_0$ wide; this width is the same as that used by de Silva *et al.* (2016). The peaks in these PDFs are modal velocities (U_m), which are associated with UMZs. PDFs of the modal velocities from all realisations upstream and downstream of the step change in roughness are illustrated in Fig. 6.

From Fig. 6 an important observation can be made: the modal velocities present upstream and downstream of the transition are different, and after a sufficient evolution distance ($x/\delta_0 \approx 5$ for both cases), have a distinct cross-over point near $U/U_\infty = 0.57$. This is explicit for the mesh case, but also exists for the smoother grit case although the con-

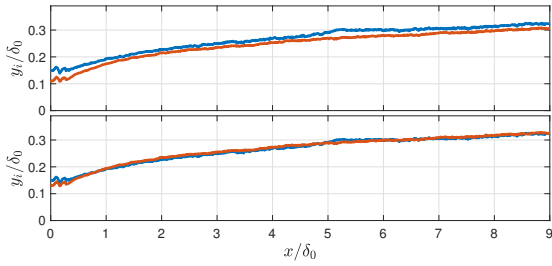


Figure 7. Average growth of the instantaneous internal layer identified by the UMZ approach for the mesh roughness: (a) as found by both method (1) and (2) described above, and (b) with method (2) adjusted by an arbitrary constant to show that it collapses with the result of method (1) when adjusted for bias.

trast between upstream and downstream of the transition is less dramatic.

The significance of the above is that there is a class of modal velocities that exist only downstream of the $S \rightarrow R$ transition, and these are a result of the change in roughness. Choosing the cross-over point as a threshold, we can then identify the UMZs associated with the roughness distinctly from those that existed over the smooth wall. We propose two ways of doing this:

- (1) Identify any modal velocity below the threshold, and then find the minimum value in the PDF between that modal velocity and the modal velocity representing the UMZ above it. Draw this contour in each image and call this the internal layer.
- (2) Draw the same contour level, which is associated with the threshold, in every image and call this the internal layer.

When using approach (1) above, a specific downstream band must be employed to identify the instantaneous inner layer modal velocity because the UMZs and modal velocities are averaged out if too long an interrogation area is selected. As such, the band spanning $5.00 \leq x/\delta_0 \leq 5.25$ is selected because it is sufficiently far downstream that in both cases the modal velocity PDFs are approximately collapsed. The instantaneous result using approach (1) is illustrated as the blue line in Fig. 2, whereby it is shown that the technique identifies an interface that exists over the roughness for most of the FOV. Applying both approaches (1) and (2) for each instantaneous realisation, and then computing the average inner layer interface position for each downstream position x/δ_0 , the mean location of the internal interface caused by the new roughness modal velocities can be determined. These mean results are illustrated in Fig. 7. From here it is evident that this internal layer grows with streamwise distance on average. In Fig. 7 it is illustrated that both methodologies produce a collapsed internal layer that differs only by a constant offset in the wall-normal direction. This result suggests a degree of robustness to the analysis as a similar result is found via two different methods. We thus proceed with method (1) because it tracks real UMZs, as opposed to method (2) where the threshold is applied without consideration of the actual modal velocities present in a snapshot.

INSTANTANEOUS INTERNAL LAYERS

For the mesh roughness, if we consider only $x/\delta_0 > 3$, the the instantaneous inner layer and the mean profile inflection point that is closer to the wall have power law exponents of $\alpha = 0.23$ and 0.22 , respectively. This suggests that after some initial equilisation distance, the two methods are tracking the same phenomenon. The growth rate of the instantaneous inner layer is slightly faster for the grit case, with $\alpha = 0.32$, but it is difficult to compare this to a fit of the inner inflection point in the mean profile because of the scatter in the latter data. A comparison between all inner layer detection methodologies is provided in Fig. 5, where qualitatively it appears that the grit instantaneous layer and the inner inflection point appear to roughly agree.

For comparison, it is important to relate the values of the present inner layer growth rates to those available in the literature. Both Cheng & Castro (2002) and Lee (2015) tracked the equilibrium layer in their studies, finding that $\alpha = 0.37$ and 0.38 , respectively. This is close to, but different from that found here. The disparity in the results can be attributed to a few factors. First, the definitions used by Cheng & Castro (2002) and Lee (2015) to track the inner layer were somewhat more arbitrary than that presented here. Their definition for the equilibrium layer was that it was the point where the mean streamwise velocity is 101% of its value for downstream roughness at the same position. This idea is predicated on the assumption that the equilibrium layer is approximately 10% of the inner boundary layer. Moreover, the change in roughness differs substantially between the cases, i.e., $\Delta h/\delta_{99,0} = 0.03, 0.045, 0.1$ for Cheng & Castro (2002), Lee (2015), and the present study, respectively. The idea that the α increases with a decrease in Δh across the step change in roughness is supported by the present results whereby α is greater for the grit compared to the mesh even though Δh for the grit is approximately half of that for the mesh. Thus, it is unsurprising that there are some quantitative differences in the identified growth rates between the present and previous studies. Nonetheless, this does not supersede the fact that the inner inflection point in the mean velocity profile appears to track with the the instantaneous inner layer found here.

The analysis thus suggests that the modal velocity detected interface is associated with the internal equilibrium layer, at least after some initial development distance ($x/\delta_0 \gtrsim 1$). The significance of this statement should not be understated. There has previously been no means by which the equilibrium layer could be tracked instantaneously. Doing so provides its mean location with more certainty, and provides additional statistics including the variability in its position and the ability to track conditional statistics across the interface. The standard deviation of the internal interface position is plotted versus its local mean position and δ_0 in Fig. 8. It can be seen that the relative fluctuations in the interface location is constant for the mesh case, while they are still approaching their steady state for the grit case, suggesting that the mesh case is farther through its evolution in a shorter distance. A local minimum is present in the curve at the location of the band used to identify the modal velocity of the inner layer, i.e., $5.00 \leq x/\delta_0 \leq 5.25$, which is logical because this is the band whereby the modal velocity is actually present, and thus the variation in the interface here is lower. The conditionally averaged streamwise velocity at the instantaneous interface location is shown for the two cases in Fig. 9. Both cases illustrate that a velocity jump exists across the interface, and that the magnitude of

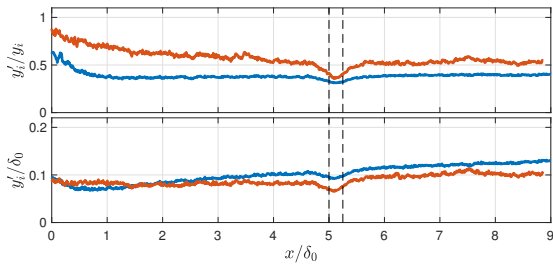


Figure 8. Standard deviation of the location of the instantaneous inner layer normalised by (top) its mean position for a given x , and (bottom) the incoming boundary layer thickness. The blue and red lines represent the mesh and grit cases, respectively. The vertical dashed lines represent the band from which the modal velocity of the inner layer is calculated.

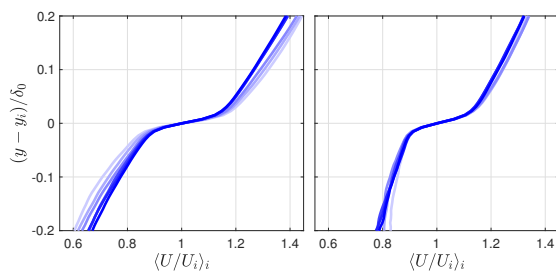


Figure 9. Conditional averages of the mean streamwise velocity across the instantaneous inner interface for the (left) mesh and (right) grit cases. Curves are generated for $0.25\delta_0$ windows from $x/\delta_0 = 2$ to 8 from lightest to darkest.

this jump decreases with downstream position. The size of the velocity jump is larger for the mesh case, which also has the physically larger internal layer.

CONCLUSIONS

As flow passes over a step change in wall roughness, inner layers form within the boundary layer and develop until the boundary layer has reached a new equilibrium with its boundary condition. This phenomenon was investigated for a smooth-to-rough transition via PIV measurements over a $\sim 11\delta_0$ FOV using two different downstream roughness topologies. For the first time, an instantaneous criterion is given to identify an internal layer that statistically resembles the equilibrium layer that forms adjacent to the wall after a step change. This methodology is based on identifying UMZs that are a result of the roughness by comparing modal velocity PDFs upstream and downstream of the step change. The ability to instantaneously describe the inner layer allows for access to a variety of flow physics that could not previously be assessed, for example: the variation in the location of the inner layer and conditional averages across the inner layer. In particular, it is demonstrated that after sufficient evolution distance, the variation in the interface location relative to its mean position is constant and that the velocity jump across the interface appears to asymptote. Interestingly, using different roughness appears to affect how quickly the interface-averaged conditional statistics become self-similar as well as the growth rate of the internal layer. Specifically, for a smaller change in roughness height across the step, the growth rate of the internal layer is faster and the

conditional statistics become self-similar earlier.

REFERENCES

- Antonia, R. A. & Luxton, R. E. 1971a The response of a turbulent boundary layer to a step change in surface roughness. Part 1. Smooth-to-rough. *J. Fluid Mech.* **48** (4), 721–761.
- Antonia, R. A. & Luxton, R. E. 1971b The response of a turbulent boundary layer to an upstanding step change in surface roughness. *J. Basic Engng.* **93**, 22–32.
- Antonia, R. A. & Luxton, R. E. 1972 The response of a turbulent boundary layer to a step change in surface roughness. Part 2. Rough-to-smooth. *J. Fluid Mech.* **53** (4), 737–757.
- Birch, D. M. & Morrison, J. F. 2011 Similarity of the streamwise velocity component in very-rough-wall channel flows. *J. Fluid Mech.* **668**, 174–201.
- Bou-Zeid, E., Meneveau, C. & Parlange, M. B. 2004 Large-eddy simulation of neutral atmospheric boundary layer flow over heterogeneous surfaces: Blending height effective surface roughness. *Water Resour. Res.* **40** (W02505).
- Chauhan, K., Philip, J., de Silva, C. M., Hutchins, N. & Marusic, I. 2014 The turbulent/non-turbulent interface and entrainment in a boundary layer. *J. Fluid Mech.* **742**, 119–151.
- Cheng, H. & Castro, I.P. 2002 Near-wall flow development after a step change in surface roughness. *Boundary-Layer Meteorol* **105**, 411–432.
- de Silva, C. M., Hutchins, N. & Marusic, I. 2016 Uniform momentum zones in turbulent boundary layers. *J. Fluid Mech.* **786**, 309–331.
- de Silva, C. M., Philip, J., Hutchins, N. & Marusic, I. 2017 Interfaces of uniform momentum zones in turbulent boundary layers. *J. Fluid Mech.* **820**, 451–478.
- Dupont, S. & Brunet, Y. 2009 Coherent structures in canopy edge flow: a large-eddy simulation study. *J. Fluid Mech.* **630**, 93–128.
- Elliott, W.P. 1958 The growth of the atmospheric internal boundary layer. *Trans. Am. Geophys.* **39** (6), 1048–1054.
- Hanson, R. E. & Ganapathisubramani, B. 2016 Development of turbulent boundary layers past a step change in wall roughness. *J. Fluid Mech.* **795**, 494–523.
- Hearst, R. J. & Ganapathisubramani, B. 2015 Quantification and adjustment of pixel-locking in Particle Image Velocimetry. *Exp. Fluids* **56** (10), 191.
- Lee, J.H. 2015 Turbulent boundary layer flow with a step change from smooth to rough surface. *Int. J. Heat Fluid Fl.* **54**, 39–54.
- Meinhart, C. D. & Adrian, R. J. 1995 On the existence of uniform momentum zones in a turbulent boundary layer. *Phys. Fluids* **7** (4), 694–696.
- Pendergrass, W. & Arya, S.P.S. 1984 Dispersion in neutral boundary layer over a step change in surface roughness: I. Mean flow and turbulence structure. *Atmos. Environ.* **18**, 1267–1279.
- Rodríguez-López, E., Bruce, P. J. K. & Buxton, O. R. H. 2015 A robust post-processing method to determine skin friction in turbulent boundary layers from the velocity profile. *Exp. Fluids* **56** (4), 68.
- Rouhi, A., Chung, D. & Hutchins, N. 2019 Direct numerical simulation of open-channel flow over smooth-to-rough and rough-to-smooth step changes. *J. Fluid Mech.* **866**, 450–486.